Chinese Chemical Letters 33 (2022) 920–925

Contents lists available at ScienceDirect

Chinese Chemical Letters

journal homepage: www.elsevier.com/locate/cclet

A binder-free electrode for efficient H_2O_2 formation and Fe^{2+} regeneration and its application to an electro-Fenton process for removing organics in iron-laden acid wastewater

Ziliang Wei, Haolin Xu, Zhenchao Lei, Xiaoyun Yi, Chunhua Feng*, Zhi Dang

The Key Lab of Pollution Control and Ecosystem Restoration in Industry Clusters, Ministry of Education, School of Environment and Energy, South China University of Technology, Guangzhou 510006, China

ARTICLE INFO

Article history:
Received 17 May 2021
Revised 16 June 2021
Accepted 2 July 2021
Available online 13 July 2021

Keywords:
Binder-free electrode
Oxygen reduction reaction
N-doped carbon nanotubes
Fe^{2+} regeneration
Acid wastewater treatment

ABSTRACT

The electro-Fenton process, with its capacity for *in-situ* H_2O_2 formation and Fe^{2+} regeneration, is a striking alternative to the traditional chemical-Fenton process. However, the frequent requirement of extra binders for electrode fabrication leads to low catalyst utilization, a complex fabrication process, and weak conductivity. Herein, a three-dimensional (3D) porous electrode was fabricated *in-situ* on a Ni foam (NF) substrate integrated with nitrogen-doped carbon nanotubes (N@C) derived from carbonization of zeolitic imidazolate framework-8 (ZIF-8) without any binder. The resulting 900/N@C-NF cathode (synthesized at 900 °C) was high in surface area, N content, and degree of graphitization, achieved high performance of H_2O_2 production (2.58 mg L^{-1} h^{-1} H_2O_2/mg catalyst) at -0.7 V (*vs.* SCE), and enabled prompt regeneration of Fe^{2+}. The electro-Fenton system equipped with the 900/N@C-NF cathode was effective in removing a diverse range of organic pollutants, including rhodamine B (RhB), phenol, bisphenol A (BPA), nitrobenzene (NB), and Cu-ethylenediaminetetraacetic acid (EDTA), and significantly attenuating the concentration of chemical oxygen demand (COD) in the real acid wastewater, exhibiting superior activity and stability. This binder-free and self-supporting electro-Fenton cathode was thus shown to be an attractive candidate for application to wastewater treatment, particularly those rich in organics, acids, and Fe^{3+}/Fe^{2+}.

The electro-Fenton process is a promising advanced oxidation method that has recently attracted considerable attention for effective abatement of organics in wastewater [1]. Leveraging the advantages of the reaction between H_2O_2 and Fe^{2+} to produce the highly reactive oxidant $^{\bullet}OH$ (Eq. 1) [2,3], which rapidly degrades organic pollutants, the electro-Fenton process offers more benefits than the classic Fenton reaction. These include i) the *in-situ* generation of H_2O_2 from the cathode *via* two-electron reduction of oxygen (Eq. 2), which avoids the risk of transport, storage, and operation of H_2O_2; ii) and the regeneration of Fe^{2+} *via* cathodic reduction of Fe^{3+} (Eq. 3), which ensures the continuous supply of Fe^{2+} to enhance reaction efficiency [4]. The most suitable scenario for the application of the electro-Fenton process is the treatment of acid wastewater laden with Fe^{3+}/Fe^{2+}, because this satisfies the requirement of a low pH value and iron sources. While numerous efforts have been directed toward relevant electro-Fenton studies, tests of this process on actual acid wastewater remain relatively scarce.

$$H_2O_2 + Fe^{2+} \rightarrow Fe^{3+} + {}^{\bullet}OH + OH^- \quad (1)$$

$$O_2 + 2e^- + 2H^+ \rightarrow H_2O_2 \quad (2)$$

$$Fe^{3+} + e^- \rightarrow Fe^{2+} \quad (3)$$

A critical aspect in enhancing the overall performance of the electro-Fenton process is the development of highly efficient and active cathode materials to boost H_2O_2 yield [5]. Carbonaceous materials have been widely utilized as cathodes in H_2O_2 production owing to their good chemical stability, high electrical conductivity, reasonable level of H_2O_2-generating activity, low catalytic activity in H_2O_2 decomposition, and high hydrogen evolution potential [6]. Many attempts have been made to increase the reactivity and selectivity of carbon materials toward H_2O_2 generation by tuning their morphology and pore structure, creating intrinsic carbon defects, and introducing heteroatom dopants (*e.g.*, N, P and F) [7,8]. Along these lines, metal-organic frameworks (MOFs) have been recently demonstrated to be ideal precursors to heteroatom-doped porous carbons that offer large surface area and abundant active sites (induced by dopants and defects) favorable for the two-

* Corresponding author.
E-mail address: chfeng@scut.edu.cn (C. Feng).

https://doi.org/10.1016/j.cclet.2021.07.006
1001-8417/

electron oxygen reduction, because MOFs have well-organized pore structure and tunable elemental compositions [9]. For example, high H_2O_2 selectivity and generation yield were achieved with *N*-doped mesoporous carbon materials derived from MOFs [10–13]. It has been claimed that the mesoporous structure is conducive to mass transfer of H_2O_2, facilitating its release in a short contact time [10,11], and that the nitrogen (N) dopant can enhance the adsorption of O_2 and alter the adsorption of *OOH intermediate on carbon surfaces by triggering charge redistribution [12,13]. These features collectively favor H_2O_2 generation. In addition, MOFs can be directly coated or grown on the supportive substrate, making it feasible to fabricate binder-free electrodes upon pyrolysis under inert atmosphere [14]. This integrated electrode structure offers great advantages over polymeric binders, which not only add complexity to electrode fabrication and decrease the long-term stability of the electrode (due to the relatively weak adhesion between catalysts and the substrate), but also have reduced conductivity, blocked active sites for reactions, and increased resistance to mass transport [15]. These considerations evoke our interest in the *in-situ* synthesis of the integrated electrode toward high-efficiency H_2O_2 production derived from MOFs that are supported on a three-dimensional (3D) substrate (*e.g.*, Ni foam).

The objectives of the current study are to develop a binder-free and self-supporting electro-Fenton electrode with the capability of *in-situ* formation of H_2O_2 and regeneration of Fe^{2+}, and to corroborate the feasibility of its application to oxidizing organics in real acid wastewater. To this end, N-doped mesoporous carbon firmly supported on Ni foam (N@C-NF) was attained by a simple one-step pyrolysis of an as-prepared mixture containing zeolitic imidazolate framework-8 (ZIF-8, a MOF providing hierarchical porosity, uniform N doping, and carbon defects) and a piece of Ni foam under inert atmosphere. A variety of organic pollutants, including rhodamine B (RhB), phenol, bisphenol A (BPA), nitrobenzene (NB), and Cu-ethylenediaminetetraacetic acid (EDTA), were selected as model pollutants to evaluate the performance of the electro-Fenton process equipped with the N@C-NF system. In addition to the physicochemical characterizations of the as-obtained electrode materials, their capabilities of H_2O_2 formation and Fe^{2+} regeneration were assessed, and the role of $^{\bullet}$OH in catalysis was identified. Key factors that impact performance, such as the pyrolysis temperature and the applied cathode potential, were investigated. Furthermore, the performance of the binder-free electro-Fenton electrode for removing organic pollutants in real acid pickling wastewater and acid mining drainage (AMD) (which both contain high concentrations of Fe^{2+}/Fe^{3+}) was evaluated.

The procedures for synthesis of the binder-free 900/N@C-NF are illustrated in Fig. S1 (Supporting information). Figs. 1a–d show the surface morphology of 900/N@C-NF, in which carbon nanotube-like materials grew uniformly on the surface of the 3D NF. Fig. 1a indicates that the 3D structure was well maintained after *in-situ* catalyst deposition, implying that ZIF-8 strongly interacted with the NF. The enlarged scanning electron microscopy (SEM) image (Fig. 1b) showed that the NF surface was fully covered by the carbon nanotubes, leading to an increment of roughness and accordingly larger active surface area for the oxygen reduction reaction. The carbon nanotube framework derived from ZIF-8 was also observable in the high-resolution transmission electron-microscopy (HRTEM) image (Fig. 1c), having an average width of 90 nm. According to the elemental mapping images (Fig. 1d), C and N atoms were well dispersed on the NF surface and substantially more C was visible.

X-ray diffraction (XRD) and X-ray photoelectron spectroscopy (XPS) characterizations were conducted to obtain information on the crystalline structure and elemental composition of 900/N@C-NF. For comparisons, samples of 1000/N@C-NF and 800/N@C-NF, which pyrolyze at different temperatures, were also characterized. The XRD patterns of all of the samples (Fig. 1e) had similar features, with three sharp diffraction peaks at approximately 44.5°, 51.8° and 76.4°, assigned to the (111), (200) and (220) planes of the face-centered cubic phase of Ni, respectively [16]. This indicates that the deposition of nitrogen-doped carbon nanotubes had a negligible effect on the crystal structure of NF. Since the N content and N species distribution in the doped carbon materials play an important role in ORR catalysis [11], N 1s XPS spectra were often compared between samples. Fig. 1f shows that the N 1s XPS spectra can be deconvoluted into three well-resolved contributions, including the peak of pyridinic-N, pyrrolic-N and graphitic-N at binding energies of 398.6, 399.8 and 400.9 eV, respectively [17]. Fig. 1g indicates that increasing the temperature reduced the relative N content in the catalysts, consistent with many previous reports. Also, the pyridinic-N and graphitic-N became the dominant species at higher temperatures, which may act as the active sites for ORR in the N-doped carbon materials under acidic conditions [18]. It has been previously reported that the graphitic-N sites can donate electrons to the p-conjugated C atoms, thus causing charge redistribution to facilitate O_2 adsorption [19,20]. In addition, it has been claimed that the pyridinic N sites prompt their adjacent C atoms to be the active sites with Lewis basicity, also resulting in the promoted O_2 adsorption [21,22]. Then, the key intermediate *OOH is formed *via* one proton-coupled electron transfer. The pyridinic-N and graphitic-N are demonstrated to have the capability of reduce the adsorption energy of *OOH, which is directly released into the solution and combined with proton to form H_2O_2 [23,24].

The Raman spectra show information on the degree of graphitization for the carbon materials. For the Raman spectra of all samples (Fig. 1h), two strong absorption peaks at 1340 cm^{-1} (D peak) and 1570 cm^{-1} (G peak) were revealed. The D peak induced by the symmetrical stretching vibration of the sp^2 atomic ring is generally understood to characterize the degree of defect and disorder of carbon materials, and the G peak attributed to the sp^2 atomic bond stretching is considered indicative of the graphitization degree of carbon materials [11,25]. The I_D/I_G value decreased when the carbonization temperature increased from 800 °C to 1000 °C, suggesting an improved degree of graphitization. The specific surface area and porosity of carbon materials are important to their electrocatalytic performance for ORR, which have been evaluated based on nitrogen adsorption-desorption isotherms [26]. As shown in Figs. 1i and j, the isotherms of all samples showed similar type-IV hysteresis loops at a relatively small pressure, indicating the existence of a mesoporous structure [27]. The relevant Brunauer-Emmett-Teller (BET) surface area and total pore volume of them are summarized in Table S1 (Supporting information); it was seen that the 900/N@C-NF sample exhibited the largest surface area of 19.37 m^2/g and pore volume of 1.12 $\times$ 10^{-2} cm^3/g, and the smallest average pore diameter of 2.32 nm. In comparison to NF (0.510 m^2/g and 6.743 $\times$ 10^{-4} cm^3/g), the carbonization significantly increased surface area and total pore volume, supporting N@C-NF as a potential electrocatalyst for H_2O_2 production.

The performance of N@C-NF catalysts for H_2O_2 electro-generation through $2e^-$ ORR was verified by analyzing the amount of H_2O_2 produced from different electrolysis times, and the results are shown in Figs. 2a–d. As one can see, the pyrolysis temperature exerted negligible effect on H_2O_2 production for the bare NF; in contrast, it had a significant impact on H_2O_2 production for the N@C-NF (Fig. 2a). The 900/N@C-NF cathode achieved the best performance, with the accumulation of H_2O_2 reaching a maximum value of 46.2 mg/L within 1 h. The capacity of 900/N@C-NF for H_2O_2 electro-generation is also highly sensitive to the applied potential (*i.e.*, the driving force for cathode reduction). As the applied potential increased from –0.5 V to –0.7 V (Fig. 2b), the H_2O_2 accumulation underwent a significant rise due to the improved $2e^-$ ORR process. However, its accumulation noticeably de-

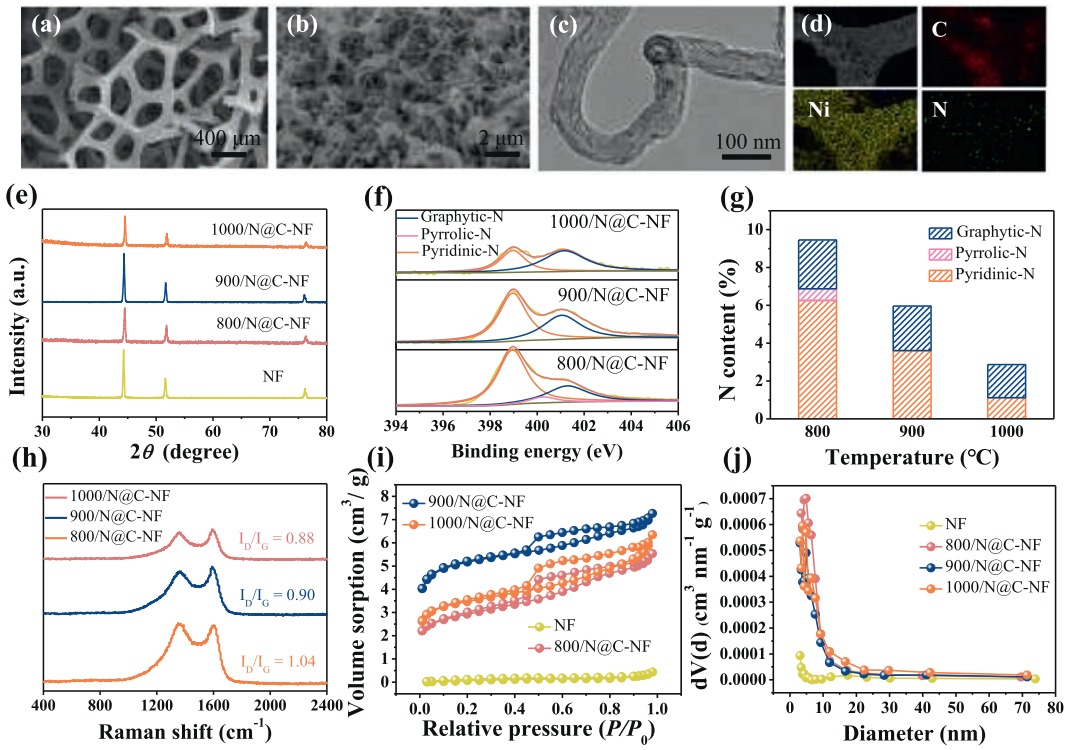

Fig. 1. (a, b) SEM images, (c) HRTEM image, and (d) element mapping of 900/N@C-NF. (e) XRD patterns, (f) N 1s XPS spectra, and (g) N content (atomic %) and N species distribution, (h) Raman spectra, (i) N_2 adsorption isotherms and (j) pore size distribution of different samples.

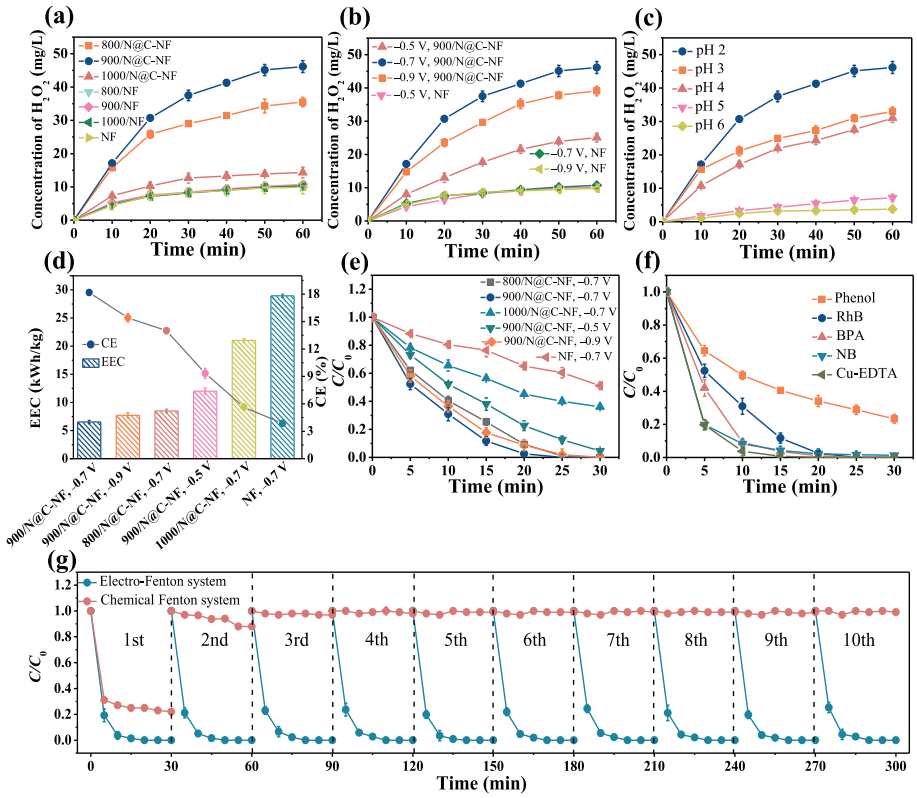

Fig. 2. Effects of (a) carbonization temperature (–0.7 V and pH 2), (b) cathode potential (pH 2), and (c) pH (–0.7 V and 900/N@C-NF cathode) on H_2O_2 production at different cathodes. (d) The corresponding EEC and CE were calculated from different cathode systems. (e) Time courses of RhB concentration as a function of different cathode systems (pH 2, initial [RhB] = 20.0 mg/L, and [Fe^{3+}] = 0.1 mmol/L). (f) Time courses of concentrations of different pollutants in the electro-Fenton system (pH 2, –0.7 V, 900/N@C-NF cathode, initial [pollutant] = 20.0 mg/L, and [Fe^{3+}] = 0.1 mmol/L). (g) Repeatable tests of RhB degradation in the electro-Fenton system (pH 2, –0.7 V, 900/N@C-NF cathode, initial [RhB] = 10.0 mg/L, and [Fe^{3+}] = 0.1 mmol/L) and the chemical Fenton system (pH 2, [H_2O_2] = 46.2 mg/L, initial [RhB] = 10.0 mg/L, and [Fe^{2+}] = 0.1 mmol/L).

creased when the potential was further increased to –0.9 V. This phenomenon is consistent with results from the literature [28], and considered to be resulted from the $4e^-$ ORR (Eq. 4), hydrogen evolution reaction (HER) (Eq. 5), and/or decomposition of H_2O_2 (Eq. 6). Meanwhile, the H_2O_2 electro-generation at the bare NF did not vary when the cathode potential changed from –0.5 V to –0.9 V. The effect of pH on H_2O_2 electro-generation on the 900/N@C-NF cathode was investigated at a potential of –0.7 V. In Fig. 2c, when the solution pH rose from 2.0 to 6.0, the H_2O_2 yield substantially declined. This might be due to the significant decrease in the amount of H^+ that was an essential factor for H_2O_2 production (Eq. 2). The observation is consistent with the literature reports [7,25], as the participation of H^+ could facilitate the proton-coupled electron transfer process for H_2O_2 generation.

$$O_2 + 4H^+ + 4e^- \rightarrow 2H_2O \quad (4)$$

$$2H^+ + 2e^- \rightarrow H_2 \quad (5)$$

$$2H_2O_2 \rightarrow 2H_2O + O_2 \quad (6)$$

In addition, the current efficiencies and energy efficiencies of different catalysts at different cathode potentials were calculated and compared. The 900/N@C-NF cathode at the cathode potential of –0.7 V exhibited better performance in terms of higher current efficiency (18.18%) and lower electric energy consumption (6.52 kWh/kg) after 1 h of operation (Fig. 2d). A significant result is that the binder-free 900/N@C-NF cathode outperforms the mostly reported binder-available cathodes with respect to a larger amount of H_2O_2 production per mg of catalyst compared to values from the literature (Table S2 in Supporting information). This is the consequence of the high catalyst utilization offered by the integrated electrode, as the electrodes with the use of binders usually suffer problems in reduction in conductivity, blocking of the active sites, and poor mass transport [15]. As a result, the 900/N@C-NF cathode also required lower electric energy consumption for the production of the same amount of H_2O_2.

The performance of the electro-Fenton system equipped with the N@C-NF cathodes was evaluated with different pollutants. Taking RhB as an example, the effects of pyrolysis temperature and applied cathode potential on its conversion were investigated. As shown in Fig. 2e, RhB with an initial concentration of 20 mg/L can be completely removed within 25 min on the 900/N@C-NF cathode at –0.7 V. Likewise, total removal of RhB was achieved within 30 min on the 900/N@C-NF cathode at –0.9 V or the 800/N@C-NF cathode at –0.7 V. The conversion rate within 30 min was 95.4% and 63.9%, in relation to the 900/N@C-NF cathode at –0.5 V and the 1000/N@C-NF cathode at –0.7 V, respectively. The electro-Fenton system with a bare NF cathode at –0.7 V allowed for removal of only 48.7% of RhB. Their corresponding apparent rate constants for RhB removal were calculated to be 0.14, 0.11, 0.091, 0.065, 0.038, and 0.018 min^{-1} for the 900/N@C-NF (–0.7 V), 900/N@C-NF (–0.9 V), 800/N@C-NF (–0.7 V), 900/N@C-NF (–0.5 V), 1000/N@C-NF (–0.7 V) and NF (–0.7 V) electrodes, respectively (Fig. S2 in Supporting information). Note that the decreasing trend was highly correlated with the order of the amount of H_2O_2 electro-generation, confirming that H_2O_2 production capacity is the key to boosting performance of the electro-Fenton system. This capacity is closely correlated to the content of pyridinic-*N* and graphitic-*N*, and surface area of carbon catalysts [18,19].

The versatility of the electro-Fenton system integrated with the 900/N@C-NF cathode was evaluated with different kinds of pollutants, including phenol, BPA, NB, and Cu-EDTA. The effectiveness of this cathode for removing a variety of these compounds is shown in Fig. 2f. BPA, NB and Cu-EDTA completely disappeared within 30 min and the percentage of phenol removal was 76.7%. The detection of the variation in the total organic carbon (TOC) as a function of time (Fig. S3 in Supporting information) indicated that 39.1%, 32.8%, 63.9%, 43.8%, and 19.2% of TOC was removed within 30 min, corresponding to phenol, RhB, BPA, NB, and Cu-EDTA treatments, respectively. These results affirm that the binder-free 900/N@C-NF cathode is effective in degrading different organic pollutants, showing promise for treating organic acid wastewater.

The long-term stability of the 900/N@C-NF cathode, a critical factor toward the real application of the electrocatalysts, was investigated. Because of the capability of the electro-Fenton system to regenerate Fe^{2+} from cathodic reduction of Fe^{3+}, only 0.1 mmol/L Fe^{3+} was added the first time. As clearly shown in Fig. 2g, there was insignificant decay in the reaction kinetics of RhB degradation after being used 10 times. The apparent rate constants were 0.29 and 0.25 min^{-1} for the first and tenth cycles, respectively (Fig. S4 in Supporting information); the small change reflects excellent stability and performance in the 900/N@C-NF electrode. The 900/N@C-NF cathode also exhibited good cycling stability when used for degradation of other pollutants such as NB and BPA (Fig. S5 in Supporting information). For comparison, a traditional Fenton process with the addition of 46.2 mg/L H_2O_2 was run for destructing RhB and only 78% of RhB was removed during the first cycle. The poor performance can be attributed to the inability to continuously produce H_2O_2 and the difficulty in Fe^{2+} regeneration. For the same reasons, the degradation performance deteriorated seriously with each additional cycle. The SEM and HRTEM images of the 900/N@C-NF cathode after 10-cycle electro-Fenton tests were presented in Fig. S6 (Supporting information). It can be clearly seen that the cycling tests did not alter the 3D structure (Fig. S6a), and that the carbon nanotubes were still present on the NF surface (Fig. S6b). The hollow tubular structure of carbon nanotubes was revealed in the HRTEM images (Figs. S6c and d) after 10-cycle reaction, which was similar to that observed before reaction. The invariability of the morphological structure of the sample further supported its good stability for repeatable operations.

The inefficient Fe^{3+}/Fe^{2+} cycle has been considered to be the critical obstacle to the efficiency of traditional Fenton reaction, in which Fe^{2+} is rapidly depleted and regeneration of Fe^{2+} by the reaction between Fe^{3+} and H_2O_2 is kinetically unfavorable [29]. The electro-Fenton process can overcome this drawback because of the cathode-driven Fe^{2+} regeneration, which thus ensures the continuous production of radicals. Despite the possibility of cathodic reduction of Fe^{3+} to Fe^{2+}, the reaction kinetics is highly dependent on the cathode material. The capacity of the 900/N@C-NF cathode to regenerate Fe^{2+} was thus evaluated. Fig. 3a compares the time courses of phenol concentration for the three consecutive cycles between the electro-Fenton process and the traditional Fenton process. Analogous to the degradation of RhB, there were insignificant variations in the rate of phenol oxidation between three cycles of operation in the electro-Fenton process, whereas a substantial rate decline was observed in the chemical Fenton process. An interesting detail in Fig. 3b shows that the electro-Fenton system with the 900/N@C-NF cathode allowed rapid production of Fe^{2+}, indicating fast Fe^{3+} to Fe^{2+} kinetics. The slight decrease in the Fe^{2+} concentration late in the first cycle was due to the competitive reaction between Fe^{2+} and $^{\bullet}OH$ (Eq. 7) [30], when the majority of organic pollutants are eliminated. The concentration of Fe^{2+} immediately rose once fresh phenol was added, and it remained relatively constant for the remaining time. In contrast, the amount of Fe^{2+} continually dropped during the chemical Fenton process. It can be inferred that the prompt regeneration of Fe^{2+} is essential for the superior performance of the electro-Fenton system (with the 900/N@C-NF cathode) over the chemical-Fenton system.

$$Fe^{2+} + {}^{\bullet}OH \rightarrow Fe^{3+} + OH^- \quad (7)$$

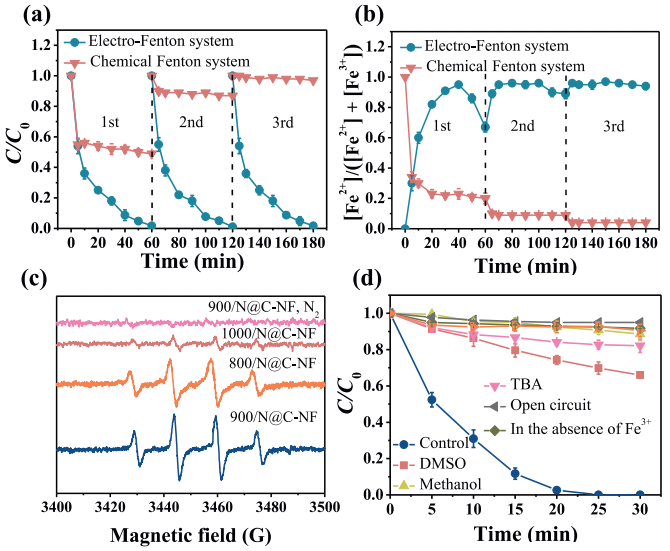

Fig. 3. (a) Repeatable tests of phenol degradation in the electro-Fenton system (pH 2, 900/N@C-NF cathode, initial [phenol] = 10.0 mg/L, and $[Fe^{3+}]$ = 0.1 mmol/L) and the chemical Fenton system (pH 2, $[H_2O_2]$ = 46.2 mg/L, initial [phenol] = 10.0 mg/L, and $[Fe^{2+}]$ = 0.1 mmol/L). (b) Time courses of Fe^{2+} concentration/(Fe^{2+} concentration + Fe^{3+} concentration) in the electro-Fenton system and the chemical Fenton system. (c) DMPO-probed EPR spectra for different systems. (d) Time courses of RhB concentration in the presence of different scavengers or under the conditions of open-circuit and the absence of Fe^{3+}. Experimental conditions: pH 2, 900/N@C-NF cathode, initial [RhB] = 20.0 mg/L, and $[Fe^{3+}]$ = 0.1 mmol/L).

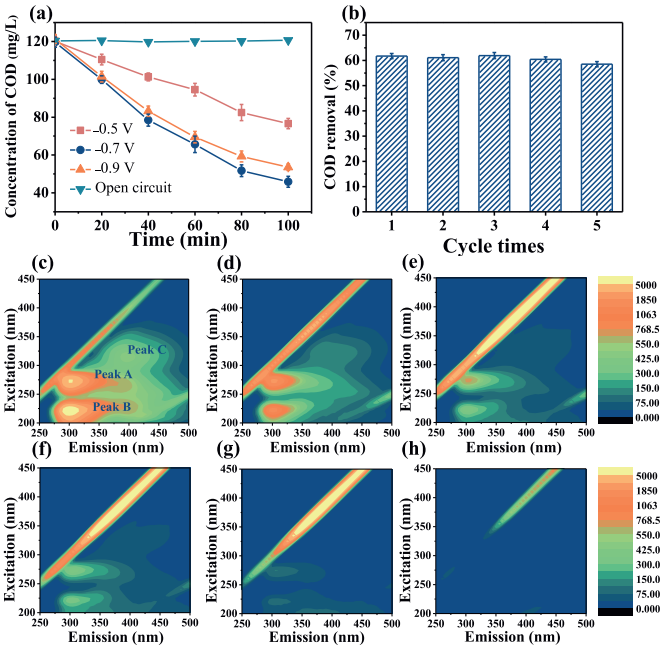

Fig. 4. Time courses of COD concentration in the pickling wastewater treated by the electro-Fenton process with the 900/N@C-NF cathode: (a) Effect of applied potential; and (b) Repeatable tests at –0.7 V. No external chemicals (like Fe^{2+}, Fe^{3+}, H_2O_2, and acids) were added. Variations in the EEM fluorescence spectra of pickling wastewater (c) before and after electro-Fenton treatment over (d) 20 min, (e) 40 min, (f) 60 min, (g) 80 min and (h) 100 min at –0.7 V.

The electron para-magnetic resonance (EPR) tests using DMPO as a spin-trapping agent were performed to identify the reactive species generated in the electro-Fenton systems. As shown in Fig. 3c, the EPR spectra of the electro-Fenton processes with the N@C-NF cathodes exhibited quaternary peaks characteristic of DMPO-OH adducts (h_{fsc} of $\alpha_N = \alpha_H$ = 14.9 G), which is generally assigned to the production of $^{\bullet}OH$ [28,31–33]. The intensity of the peaks generated by the 900/N@C-NF cathode in the O_2-saturated solution is higher than counterparts of other cathodes, an indication of the higher $^{\bullet}OH$ yield. The order of $^{\bullet}OH$ generation among these cathode materials was 900/N@C-NF > 800/N@C-NF > 1000/N@C-NF, which coincides with the order of the reaction kinetics of pollutant degradation. This verifies the role of $^{\bullet}OH$ in catalysis. In the scenario of an O_2-free solution (the cell purged with N_2), there were no EPR signals corresponding to radical peaks, indicating that the generation of $^{\bullet}OH$ mainly stems from H_2O_2 produced by $2e^-$ ORR.

Quenching experiments were further performed to clarify the role of $^{\bullet}OH$ in facilitating pollutant oxidation and to distinguish the contribution of $^{\bullet}OH_{ads}$ (adsorbed on the electrode surface) and $^{\bullet}OH_{free}$ (dissolved in the solution). It has been reported that TBA and DMSO can be used as scavengers, quenching $^{\bullet}OH_{free}$ and $^{\bullet}OH_{ads}$, respectively [34,35]. Moreover, methanol can serve as a scavenger for both $^{\bullet}OH_{free}$ and $^{\bullet}OH_{ads}$ [34]. Prior to these tests, two reference tests of pollution adsorption and direct oxidation by H_2O_2 were performed under the conditions of open circuit and absence of Fe^{3+}, respectively. Fig. 3d shows that only 5.0% of RhB was lost by adsorption and 8.3% of RhB was removed by H_2O_2 oxidation after 30 min of operation, indicating their small contributions to pollutant removal. The remarkable retardment of the reaction was observed in Fig. 3d as a result of the addition of scavengers. When TBA was added, an obvious quenching effect was apparent with only 17.8% of RhB removed after 30 min, suggesting that $^{\bullet}OH_{free}$ plays a significant role in oxidation. DMSO also quenches the reaction (34% of RhB disappeared after 30 min), indicating that $^{\bullet}OH_{ads}$ might also have a role in oxidizing pollutants, but a less significant one than that of $^{\bullet}OH_{free}$. Also, the addition of methanol dramatically reduced the removal rate of RhB; 30 min of electrolysis only resulted in removal percentage of 11.5%, again confirming that both $^{\bullet}OH_{ads}$ and $^{\bullet}OH_{free}$ are responsible for removal of RhB.

The application of the electro-Fenton system integrated with the binder-free 900/N@C-NF cathode to removing organic pollutants was tested with real acid wastewater laden with Fe^{3+}/Fe^{2+}. Pickling wastewater (resulting from cleanup of oil- and rust-contaminated metal surfaces by chemicals) has low pH, high concentrations of Fe^{2+} and Fe^{3+}, and includes organic pollutants (see Table S3 in Supporting information for the detailed information of its composition). It was accordingly chosen as the subject of investigation. Fig. 4a shows that disconnection of the circuit did not allow reduction in COD concentration, and that application of the cathode potential distinctly abated COD. As the potential increased from –0.5 V to –0.7 V, the percentage of COD removal after 100 min of operation increased from 36.2% to 61.7%. A further increase in the cathode potential from –0.7 V to –0.9 V resulted in a slow decrease in the reaction rate. Such dependence on the cathode potential agrees well with the above-mentioned results. The 900/N@C-NF cathode also exhibited outstanding longevity for real wastewater treatment. As illustrated in Fig. 4b, the electrocatalytic activity of the 900/N@C-NF cathode was retained well, as the percentage of COD removal was maintained in a narrow range from 58.5% to 61.9% for the consecutive five-cycle operation. The decay in the fluorescence signals as a function of time (Figs. 4c–h) further verified the abatement of organic matter in the pickling wastewater. As reported, the emission/excitation maxima located at around 305/270 nm (Peak A) and 400/330 nm (Peak C) are indicative of the presence of lubricating oil and diesel oil [36], and those at 305/220 nm (Peak B) are associated with simple aromatic proteins such as tyrosine [37]. The fluorescence peaks gradually weakened with increasing electrolysis time and completely disappeared after 100 min of operation. These results corroborate that the electro-

Fenton system is capable of removing the organic substances available in the acid pickling wastewater.

Another typical acid wastewater laden with Fe^{3+}/Fe^{2+} is the AMD (see Table S4 in Supporting information for the detailed information of its composition) produced by the oxidative dissolution of sulfide minerals [38]. Because of the possibility of flotation effluents being mixed with AMD in some cases, eliminating organic matter is necessary in treating the mixed wastewater. It was apparent from Fig. S7 (Supporting information) that the electro-Fenton system with the 900/N@C-NF cathode can successfully attenuate the amount of COD in the AMD (external phenol was added to mimic the organic pollutants contained in flotation effluents). Note that neither extra Fe^{3+}/Fe^{2+} nor acids were supplemented during treatment of pickling wastewater or AMD. Both case studies provide compelling evidence that the electro-Fenton process with a binder-free cathode is fully capable of removing organics in iron-laden acid wastewater.

In this work, we successfully synthesized a binder-free and self-supporting electro-Fenton cathode, in which N-doped mesoporous carbon nanotubes derived from ZIF-8 were integrated on the Ni foam substrate. The 900/N@C-NF electrode featured a large surface area, was rich in pyridinic-N and graphitic-N, had a high degree of graphitization, and exhibited outstanding performance in terms of *in-situ* formation of H_2O_2 and regeneration of Fe^{2+}. The electro-Fenton system with the 900/N@C-NF cathode was here shown to be capable of degrading a variety of pollutants such as RhB, phenol, BPA, NB, and Cu-EDTA, showing high activity and good longevity. Furthermore, this cathode was found to be effective in eliminating organic pollutants available in real acid pickling wastewater and acid mining drainage, without the addition of external H_2O_2 and Fe^{3+}/Fe^{2+}. These findings demonstrate that binder-free electro-Fenton cathodes show promise in application to acid wastewater treatment.

Declaration of competing interest

The authors declare that they have no known competing financial interests or personal relationships that could have appeared to influence the work reported in this paper.

Acknowledgments

We gratefully acknowledge financial support from the Guangdong Special Support Plan for Innovation Teams (No. 2019BT02L218); the Science and Technology Planning Project of Guangdong Province, China (No. 2019A050510009); the Guangdong Special Support Plan for Young Top-notch Talents (No. 2019TQ05L179); the National Natural Science Foundation of China (No. 21876052); the Science and Technology Program of Guangzhou, China (No. 201904010293); and the Fundamental Research Funds for the Central Universities, SCUT (No. 2020ZYGXZR055).

Supplementary materials

Supplementary material associated with this article can be found, in the online version, at doi:10.1016/j.cclet.2021.07.006.

References

[1] C. Chen, Y. Zhu, M. Tian, et al., Nano Energy 81 (2021) 105623.
[2] C. Trellu, M. Rivallin, S. Cerneaux, et al., Chem. Eng. J. 400 (2020) 125936.
[3] C. Wang, Y. Liu, T. Zhou, et al., Chin. Chem. Lett. 30 (2019) 2231–2235.
[4] S. Lanzalaco, I. Sirés, M.A. Sabatino, et al., Electrochim. Acta 246 (2017) 812–822.
[5] S. Ganiyu, M.J.G.D. Araújo, E.C.T.D.A. Costa, J.E. Santos, S.B.C. Pergher, Appl. Catal. B: Environ. 238 (2020) 119652.
[6] X. Shen, F. Xiao, H. Zhao, et al., Environ. Sci. Technol. 54 (2020) 4564–4572.
[7] K. Zhao, Y. Su, X. Quan, et al., J. Catal. 357 (2018) 118–126.
[8] Y. Xia, H. Shang, Q. Zhang, Y. Zhou, X. Hu, J. Electroanal. Chem. 840 (2019) 400–408.
[9] K. Liu, M. Yu, H. Wang, et al., Environ. Sci. Technol. 53 (2019) 6474–6482.
[10] D. Zhang, T. Liu, K. Yin, C. Liu, Y. Wei, Chem. Eng. J. 383 (2020) 123184.
[11] X. Sheng, N. Daems, B. Geboes, et al., Appl. Catal. B: Environ. 176-177 (2015) 212–224.
[12] Y. Jiang, P. Ni, C. Chen, et al., Adv. Energy Mater. 8 (2018) 1801909.
[13] Y. Sun, I. Sinev, W. Ju, et al., ACS Catal. 8 (2018) 2844–2856.
[14] L. Zhang, Y. Ding, R. Li, et al., J. Mater. Chem. B 5 (2017) 5549–5555.
[15] F. Li, J. Du, X. Li, et al., Adv. Energy Mater. 8 (2018) 1702598.
[16] W. Liu, Q. Shao, G. Ji, et al., Chem. Eng. J. 313 (2017) 734–744.
[17] Y. Cao, W. Si, Q. Hao, et al., Electrochim. Acta 261 (2018) 206–213.
[18] W. Yang, M. Zhou, N. Oturan, et al., Electrochim. Acta 297 (2019) 582–592.
[19] J. Zhang, G. Zhang, S. Jin, et al., Carbon 163 (2020) 154–161.
[20] E. Contreras, D. Dominguez, H. Tiznado, et al., Nanoscale 11 (2019) 2829–2839.
[21] D. Guo, R. Shibuya, C. Akiba, et al., Science 351 (2016) 361–365.
[22] H. Shao, Q. Zhuang, H. Gao, Y. Wang, et al., Inorg. Chem. Front. 8 (2021) 173–181.
[23] M. Qin, S. Fan, L. Wang, et al., J. Coll. Interface Sci. 562 (2020) 540–549.
[24] Y. Sun, S. Li, Z.P. Jovanov, et al., ChemSusChem 11 (2018) 3388–3395.
[25] Y. Liu, X. Quan, X. Fan, H. Wang, S. Chen, Angew. Chem. Int. Ed. 54 (2015) 6837–6841.
[26] F. Yu, L. Tao, T. Cao, Environ. Pollut. 255 (2019) 113119.
[27] J. Qu, T. Che, L. Shi, Q. Lu, S. Qi, Chin. Chem. Lett. 30 (2019) 1198–1203.
[28] W.L. Jiang, X. Xia, J.L. Han, et al., Environ. Sci. Technol. 52 (2018) 9972–9982.
[29] B. Shen, C. Dong, J. Ji, M. Xing, J. Zhang, Chin. Chem. Lett. 30 (2019) 2205–2210.
[30] Y. Gao, W. Zhu, C. Wang, et al., Electrochim. Acta 330 (2020) 135206.
[31] M.R. Haider, W.L. Jiang, J.L. Han, et al., Appl. Catal. B: Environ. 256 (2019) 117774.
[32] W. Yang, M. Zhou, L. Liang, Chem. Eng. J. 338 (2018) 700–708.
[33] C. Guo, D. Yue, S. Wang, X. Qian, Y. Zhao, Chin. Chem. Lett. 31 (2020) 1978–1981.
[34] C. Liu, Y. Min, A.Y. Zhang, et al., Water Res. 165 (2019) 114980.
[35] M. Sun, Y. Zhang, H.H. Liu, et al., Environ. Int. 131 (2019) 104977.
[36] D. Kong, Y. Cui, L. Kong, S. Wang, Spectrochim. Acta A 228 (2020) 117799.
[37] H.Y. Cui, Y. Zhao, Y.N. Chen, et al., J. Hazard. Mater. 326 (2017) 10–17.
[38] M. Dutta, N. Islam, S. Rabha, et al., J. Hazard. Mater. 389 (2020) 121851.